Adsorption (2010) 16: 47–56
DOI 10.1007/s10450-010-9216-3

PROCEEDINGS OF PBAST5

Synthesis, characterization, and adsorption kinetics of titania nanotubes for basic dye wastewater treatment

Kuen-Song Lin · Hao-Wei Cheng · Wen-Ru Chen · Chian-Fu Wu

Received: 1 August 2009 / Accepted: 5 May 2010 / Published online: 19 May 2010

Abstract Titanium dioxide has been recognized as an excellent photocatalyst material applied on many fields especially for environmental science or engineering. However, the effect of acid washing treatment on the morphology or phase and pore structures of titania nanotubes (TNs) has not still been clearly investigated. The variation of morphology, formation mechanism, phase structure, and pore structure of TN were thus characterized with FE-SEM, TEM, XRD, and N_2 BET isotherms, respectively in the present work. Titania nanotube synthesized via a simple hydrothermal chemical process formed a crystalline structure with open-ended and multiwall morphologies. The XRD patterns and N_2 BET isotherms implied that the acid washing techniques could improve the TN surface area and the pore size distribution up to 292 $m^2\ g^{-1}$ and 40–60 nm, respectively. According to EXAFS/XANES spectra, the structure of the TN is closer to the anatase specimen and much more correlated with octahedral structure. Effects of the pore structure variation on basic dye (Basic Green 5 (BG5)) adsorption by TN were discussed in the present work. Moreover, the adsorption ability, mechanisms, and kinetics of BG5 dye onto TN were also examined with the aid of model analyses of the adsorption equilibrium and kinetic data. Therefore, the potential of TN for the removal of BG5 dye contaminant from wastewaters implied that further development would be warranted.

Keywords Titania nanotube · BG5 basic dye · Hydrothermal method · Adsorption kinetics · XANES/EXAFS

K.-S. Lin (✉) · H.-W. Cheng · W.-R. Chen · C.-F. Wu
Department of Chemical Engineering & Materials Science/Fuel Cell Center, Yuan Ze University, Chung-Li 320, Taiwan, ROC
e-mail: kslin@saturn.yzu.edu.tw

1 Introduction

Dye wastewaters are recognized as difficult-to-treat pollutants and are discharged by a wide variety of sources, such as textiles, mills, printing, plants, dyestuff manufacturing, and food plants (Cassano et al. 2001; Pokhrel and Viraraghavan 2004). The color produced by minute amounts of organic dyes in water is of great concern because the color in water is aesthetically unpleasant. Moreover, they are also the major sources of water pollution, because some dyes and their degradation products may be carcinogens and toxic to human beings or mammals (Lin and Lin 2007; Lee et al. 2008). Some investigations have been conducted on the physical, chemical, and biological methods for removal of the color from dye wastewater (Ramakrishna 1997; Sun et al. 2002; Crini 2006) and it was found that physical adsorption might be an efficient and economic process to remove dyes from the wastes streams and also to control the biochemical oxygen demand (Crini 2006). The application of adsorption technology utilizing commercial activated carbon has become one of the most effective technologies for the removal of effluents of dyes (Ramakrishna 1997). However, activated carbon often suffers from high-cost production as well as regeneration. Other materials, such as some natural adsorbents, certain waste materials, and some agricultural by-products have also been investigated as alternatives (Ho et al. 2003; Mohamed 2004; Wang et al. 2006). In recent years, mesoporous molecular sieves, such as FSM-16 (Mohamed 2004), MCM-22 (Wang et al. 2006), and MCM-41 (Ho et al. 2003) have been accepted as the appropriate adsorbents for the removal of dyes from wastewater due to their unique mesoporous pore structure, high specific surface area, and pore volume. In addition, titania nanotubes (TN) derived from a hydrothermal method, possesses ion-exchange characteristics (Kasuga et al. 1999; Seo

et al. 2001; Ryuhei et al. 2005; Kasuga 2006; Weng et al. 2006; Yu et al. 2006a; Zhang et al. 2008; Niu et al. 2009) and they may also offer a special environment for the adsorption of large cations, such as basic dyes. Titania nanotubes with high specific surface area has been also studied due to its excellent catalytic activities, long-term stability, non-toxicity, and low cost (Tomoko et al. 1998; Chen et al. 2002; Uzunova-Bujnova et al. 2008; Inagaki et al. 2009). Many groups have tried to analyze the characteristics of TN, from which the synthetic mechanism was examined and the sheet folding mechanism was often assumed (Wang et al. 2002; Weng et al. 2006; Yu et al. 2006b; Lee et al. 2008; Hsieh et al. 2009; Prado and Costa 2009; Zhao et al. 2009). The effects of synthetic conditions on the microstructures of the TiO_2-derived nanotubes with the emphasis placed on the reaction time, synthesis temperature, and acid washing concentration were also investigated (Tomoko et al. 1998; Seo et al. 2001; Wang et al. 2002; Weng et al. 2006; Lee et al. 2008; Zhang et al. 2008; Wu et al. 2009; Yu et al. 2009). However, it is rare in the literature to investigate systematically the effects of acid washing treatment on the microstructures of TN.

The X-ray absorption near edge structure/extended X-ray absorption fine structure (XANES/EXAFS) spectra can provide the oxidation states and fine structures of Ti atoms in TN contributing to an advanced study for the removal of dye from wastewater (Lytle 1999). However, the fine structures of TN formation are still unclear. Therefore, the main objectives of the present study were to investigate the effects of acid washing concentration/times and calcination temperatures of the hydrothermal method on the morphology, phase and/or pore structures of TN. The variation of morphology, formation mechanism, phase structure, and pore structure of TN were thus characterized with field emission-scanning electron microscopy/energy dispersive spectroscopy (FE-SEM/EDS), transmission electron microscope (TEM), X-ray diffraction (XRD), XANES/EXAFS, and N_2 BET isotherms.

2 Experimental

2.1 Preparation of TN

Titania nanotubes was prepared using a hydrothermal process and washed by 0.1–0.01 M HCl solution (Kasuga 1999, 2006; Lee et al. 2008). The TiO_2 source was the as-synthesized anatase TiO_2 nanopowder and the particle size ranged of 30–50 nm. 1–3 g of the TiO_2 nanopowder was mixed with 60–90 mL of 10 M NaOH solution followed by hydrothermal treatment of the mixture at 150°C in a 250 mL teflon-lined autoclave for 24 h. After hydrothermal reaction, the precipitate was separated by filtration and washed with a 1 M HCl solution and distilled water until pH = 7. The washed samples were dried in a vacuum oven at 110°C for 8 h and stored in glass bottles until used.

2.2 Characterization of TN

The pore volume and surface area of TN (c.a. 292 $m^2\,g^{-1}$) were obtained by N_2 BET adsorption (Micromeritics, ASAP 2020 with the accuracy of surface area deviation within 1%). The average metal concentration of TN was measured by ICP/MS (PE-SCIEX ELAN 6100 DRC). Crystalline structures of TN were measured by XRD scanned from 5 to 80° (2θ) with a scan rate of 4° (2θ) min^{-1} and monochromatic CuK_α radiation (MAC Science, MXP18) at 30 kV and 20 mA and further identified by a computer database system (JCPDS). The morphology, particle size distribution, and microstructure of TN were also determined using FE-SEM (Hitachi S-4700 II) with a resolution of 0.1 nm. In addition, TN samples were dispersed on a carbon film supported by a copper grid for TEM observation (Model Zeiss 10C) at 100 kV.

XANES/EXAFS spectra were collected at the Wiggler beam line 16A1 at the NSRRC of Taiwan. The electron storage ring were operated with energy of 1.5 GeV and a current of 100–200 mA. The double crystal monochromators employing at either beamline selected X-rays with energy resolving power ($E/\Delta E$) better than 7000, sufficient for most XAS measurements. Data were collected in fluorescence or transmission mode with a Lytle detector (Lytle 1999) in the regions of the Ti (4966 eV) K edges at room temperature. The EXAFS function was derived from the raw absorption data through the pre-edge and post-edge background subtraction and then normalized with respect to the edge jump by using a program package AUTOBK after being k^3-weighted (k-range = 2.5–12.5 $Å^{-1}$), where k is the photoelectron wave number. All the computer programs were implemented in the software package UWXAFS 3.0. The phase shifts and backscattering amplitudes were theoretically calculated by using FEFF 8.20 code based on the crystallographic data of individual species (Lytle 1999). Simulations were carried out to demonstrate the effects of the crystalline structure of the TiO_2. Multiple scatterings were included in the calculations due to obtain the origin of the spectral characteristics of the titanium structure included with the simplification of the Debye-Waller factors.

2.3 Adsorption measurements

The basic dye BG5 ($C16H_{17}ClN_4O_2S{\cdot}(1/2)ZnCl_2$, molecular weight of 433 $g\,mol^{-1}$) was selected as a typical adsorbate to discuss the adsorption selectivity of TN in terms of the pore structure of adsorbent and molecular shape of adsorbate. Analytical grade compound from Sigma Chemical Co. (USA) was used without further purification. BG5

dye adsorption data from solution was obtained by an immersion method. The dye was first dried at 105°C for 48 h to remove moisture before using it. For adsorption experiments, 0.1 g TN was added into 100 mL of dye solution at the desired concentrations. The initial pH value of the solution was adjusted with NaOH or HCl solution. The solution and solid phase were separated by centrifugation at 8000 rpm for 25 min in a Sorvall RC-5C centrifuge. A 15-mL aliquot of the supernatant was removed and analyzed for BG5 by ultraviolet/visible (UV/Vis) spectrophotometer (Hitachi U-3310) at the wavelength of 655 and 555 nm, respectively. The adsorption capacity of dye was then calculated using the relation $Q = V\Delta C/m$, where V was the volume of the liquid phase, m was the mass of TN, and ΔC was the difference between the initial and final concentration of BG5 basic dye solutions. The effect of temperature on the adsorption data was carried out by performing the adsorption experiments at various temperatures (25, 35, and 45°C).

3 Results and discussion

3.1 Morphology of TN

The preparation of TN carried out through hydrothermal reaction including with the acid (HCl) washing process is shown from the FE-SEM and TEM microphotos in Fig. 1. A large amount of TN with a diameter of 10–30 nm and a length of several hundreds nanometers are obtained. In addition, nanotube wall thickness is generally varied in different tests with the similar crystallographic pattern is also represented in Figs. 1(a) and 1(b). Further observation indicates that the prepared titanate compounds possess uniform inner and outer diameters along their length as well as multi-layered and open-ended, in good agreement with previous reports (Ryuhei et al. 2005; Weng et al. 2006; Yu et al. 2006a; Inagaki et al. 2009).

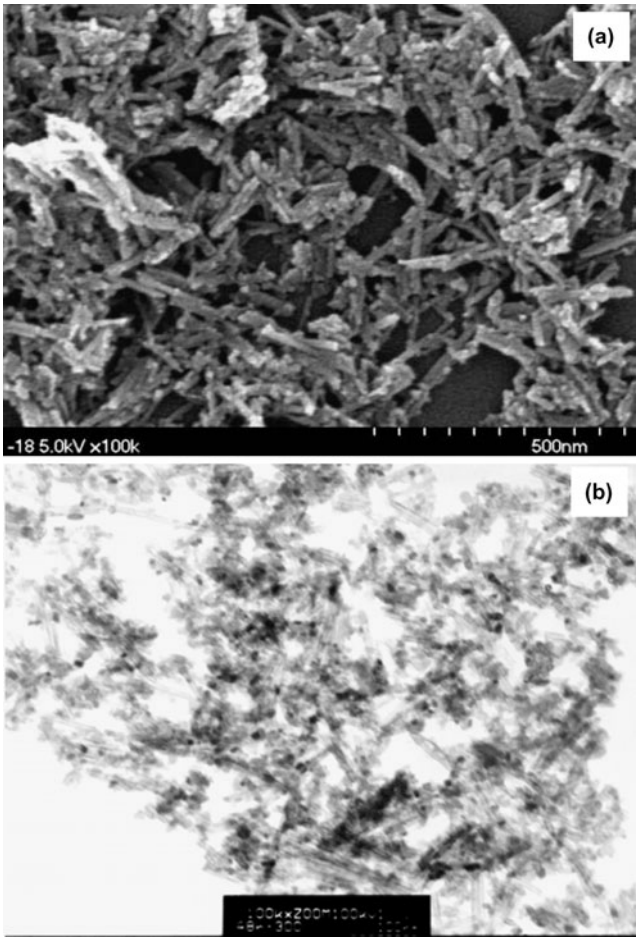

Fig. 1 (**a**) FE-SEM and (**b**) EM microphotos of TN products obtained by hydrothermal reaction and 0.1 M HCl washing using as-synthesized anatase TiO_2 nanopowder as precursors and 10 M $NaOH_{(aq)}$ at 150°C for 24 h

3.2 XRD patterns

Recent studies of the TN structure face the challenge to understand interior and the surface structures for prominent use. X-ray diffraction is a powerful technique to understand the crystal structure and size distribution. Particle size distribution and the crystalline structure of the XRD patterns for the formation of TN at 150°C were carried out at several washing conditions. The results are shown in Fig. 2. According to the reported literature (Wang et al. 2002), higher temperature (>120°C) increases the formation of microstructure of the TN. Similarly, the XRD patterns corresponding to synthesis temperatures below and above 160°C are distinct, indicating that synthesis temperature may induce a significant change in the phase structure of titanate compounds (Lee et al. 2008). Two diffraction peaks can be identified as [101] and [200] directions of the anatase phase of the TiO_2 crystal as represented in the $2\theta = 25.4$ and 48.05°, respectively, in Fig. 2(a). In addition, some other strong diffraction peak in the [004] direction are barely indentified indicated that the quasi-two dimensional lattice shell structure, included with titanate nanotube structure which is consumed after the 12 h acid washing. Moreover, TN where a lot of Na^+ existed, indicating that the remnant Na atoms stabilized the nanotube structures (Lee et al. 2008). The crystalline structure of the TN phase is observed after the 24 h acid washing to onward included the strong sustainable peak of [004] direction at the $2\theta = 37.8°$ shown in Figs. 2(b) to 2(d) (Kubo and Nakahira 2008). The anatase phase peak intensity is increased with an increase of acid washing time of the TN. The fact that most of the TN had very thin walls is confirmed from the FE–SEM/TEM analyses and the change of the peak intensity after 24 h acid washing. This indicated that the early stage of the titanate nanotube converted into TN. It is generally reported that the crystalline structure of

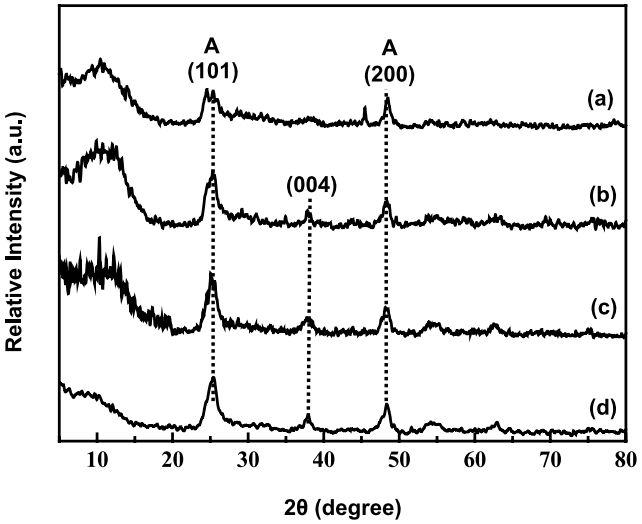

Fig. 2 XRD patterns of TN products obtained by different acid washing times of (**a**) 12, (**b**) 24, (**c**) 48, and (**d**) 60 h

the TN in the diffraction peak at 10° is belongs with $(H, Na)_2Ti_3O_7{:}xH_2O$ phase and that is consisted with our present work (Ryuhei et al. 2005; Kubo and Nakahira 2008; Wang et al. 2008). Also during the formation of TN, sodium ions play an important role. During the increasing concentration of acid washing treatment, Na^+ of the titanate nanotube is replaced with H^+ to form hydrogen titanium oxide or hydrogen titanium oxide hydrate (Kubo and Nakahira 2008). The formation of TN structure is much more stable after a 24 h acid washing process. In addition, sodium titanates probably form first from original TiO_2 through hydrothermal treatment, and then sodium titanate products change to hydrogen titanate after washed in acidic solution through an ion exchange mechanism. Therefore, the sodium ions are not substituted completely by protons after the nanotubes are washed with the $HCl_{(aq)}$ and distilled water, as can be further verified with the analysis of BET surface area and pore volume.

3.3 BET surface area and pore volume

Non-specific physical adsorption of the TN was carried out to measure the total surface area and pore size distribution, shown in Figs. 3(a) and 3(b), respectively. The surface area and pore volume calculated according to the adsorption data under different washing times are summarized in Table 1. The BJH method was employed to analyze the pore size distribution. The distribution clearly shows that the porosity of the titanate specimens is contributed by mesopores. In addition, the smaller pores (<10 nm) may correspond to the pores inside the TN and the diameters of these pores are equal to the inner diameter of the nanotubes, while the larger pores (10–100 nm) can be attributed to the voids in the aggregation of TNs (Yu et al. 2006b). The BET surface area

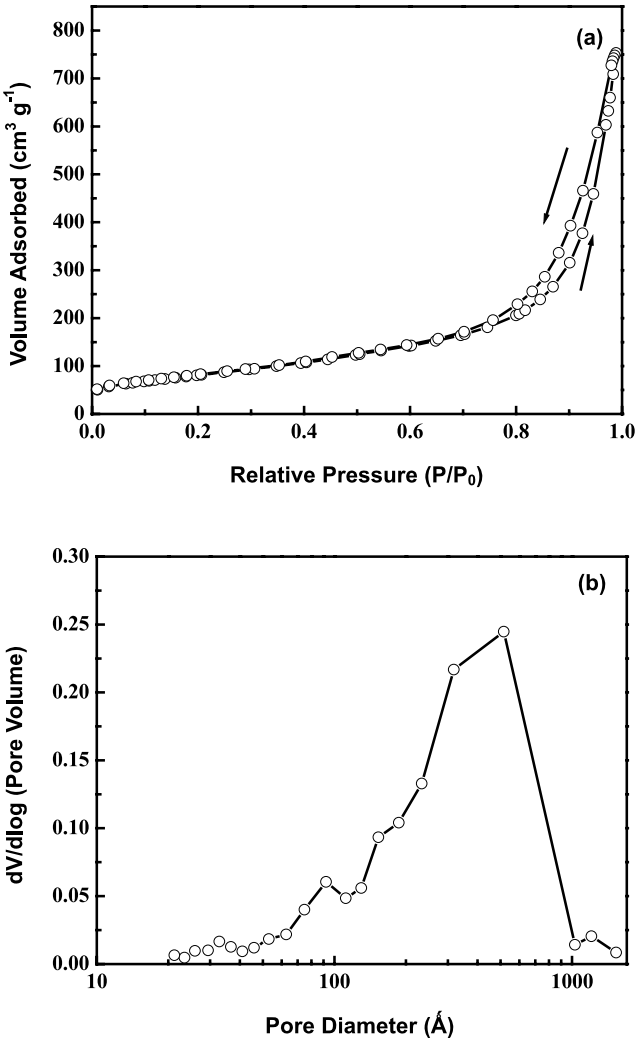

Fig. 3 (**a**) Nitrogen adsorption-desorption isotherms and (**b**) pore volumes at different pore diameters of TN products obtained under the acid washing time of 24 h at 150°C

of nitrogen adsorption was initially 277 $m^2\,g^{-1}$ and then increased slightly with the acid washing time. The highest BET surface area of 292 $m^2\,g^{-1}$ corresponded to the 24 h acid washing time. The BET surface area decreased with further acid washing of the TN. This measured data is also related with the XRD patterns represented in Fig. 2. A large surface area was generally observed for TN derived from the hydrothermal treatment of TiO_2 with NaOH, and was considered a beneficial characteristic for a great variety of applications (Tsai and Teng 2008).

The adsorption-desorption isotherms exhibit hysteresis behavior, indicating that the specimens are mainly mesoporous. Also, the type IV hysteresis isotherm is obtained and represented in Fig. 3(a) (Bond 1987; Kubo and Nakahira 2008). The adsorption hysteresis (the isotherm doesn't follow the same path in desorption as it does in adsorption) was observed in the region of a relative pressure P/P_0 above 0.6.

Table 1 Pore structure and the surface area obtained from the acid washing treatment of several period of time for TN

Acid treatment period (h)	BET surface area ($m^2\ g^{-1}$)	Pore volume ($cm^3\ g^{-1}$)
0	277.17	0.925
12	280.55	0.946
24	292.16	1.032
48	244.82	0.735

This generally occurred in the case of TN and is consistent with cylindrically shaped capillaries open at both ends (type A hysteresis loop on type IV isotherm). Condensation did not begin with increased pressure until it exceeded the effective radius of the interior (Bond 1987). Similarly, after the interior pore filled with nitrogen then the pressure decreased to a value corresponding to the minimum radius of the neck before the pore is ready to be emptied via desorption.

3.4 XANES/EXAFS analyses

Titanium oxide has distinct types of crystal structure included with the rutile and anatase. Several formats of the possible correlated titanium structure were investigated by XANES. The radial structure functions derived from the FT are shown in Figs. 4 and 5, respectively. The Ti–K edge-energy of 4965 eV was confirmed in the derivative spectra of Ti metal. The anatase phase structure of the Ti(IV) is confirmed with the edge energy at 4984.7 eV (Berry et al. 2007; Kubo and Nakahira 2008). In addition, the rutile phase intensive peak energy is split into two significant positions as 4985.2 and 4991.95 eV. An increase in relative intensity has been observed in the TiO_2 materials with increasing distortion from the octahedral TiO_6 unit, and an intense single pre-edge peak has been observed for TiO_2 with a tetrahedral geometry around Ti atom. According to previous studies, the origins of the pre-edge peaks are attributed to 1s to 3d transitions and are designated to 1s to $2t_{2g}$ and 1s to $3e_g$ transitions in an octahedral field, respectively, for the pre-edge of the phase transition of the titanium oxide structure (Kubo and Nakahira 2008). Extensive efforts have been made to theoretically calculate the pre-edge structure of TiO_2 with a limited number of atoms. The post-edge peak intensity of TNs is slightly split into the 4987.12 and 4991.25 eV and reflects the interrelated anatase and rutile phase structure (Ribeiro et al. 2007). Where as, post-edge region of the Ti K-edge XANES spectra of the anatase and TN are quite similar is represented in Fig. 4. From these results, we can affirm that the structure of the TN is closer to the anatase specimen and much more correlated with the octahedral structure.

The EXAFS bond distance r space spectra for titanium and titanium oxides particles of different diameters are

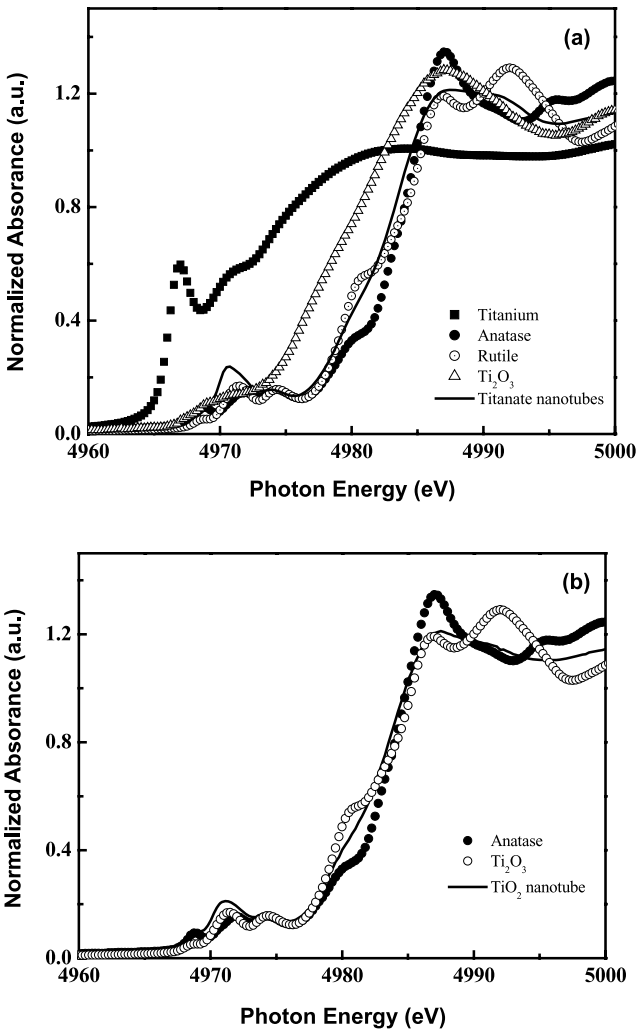

Fig. 4 XANES spectra of Ti near K-edge (4966 eV) for anatase, rutile, related Ti standards compared with (**a**) titanate nanotube and (**b**) TN

shown in Fig. 5 and Table 2. The r space data show peaks which correspond to different atomic shells around the central atom. The position of each peak is shifted slightly in r space as a result of a well-known phase shift and provides information about the relative (correlated) vibrations of the corresponding atomic shell. A reduced amplitude of a peak indicates a larger width, and hence a larger local distortion of that atomic shell. As a general trend, the oscillation amplitude in the spectra reduces as the particle size decreases. The EXAFS data (Table 2) also revealed that titanium metal possessed Ti–Ti bond distance of 2.89 Å and a coordination number of 3.98. Similarly, TN has a first shell of Ti–O bonding with a bond distance of 1.97 Å and a coordination number of 2.31. In addition, the titanate nanotubes consisted with related first shell bond distance of 1.95 Å with lower coordination number 1.98 and the highest Debye-waller factor ($\Delta\sigma^2$) with 0.0048 ($Å^2$). In all EXAFS data analyzed, the Debye-Waller factors ($\Delta\sigma^2$) were less than 0.01 Å. The apparent shortening of the Ti–O bond length probably was

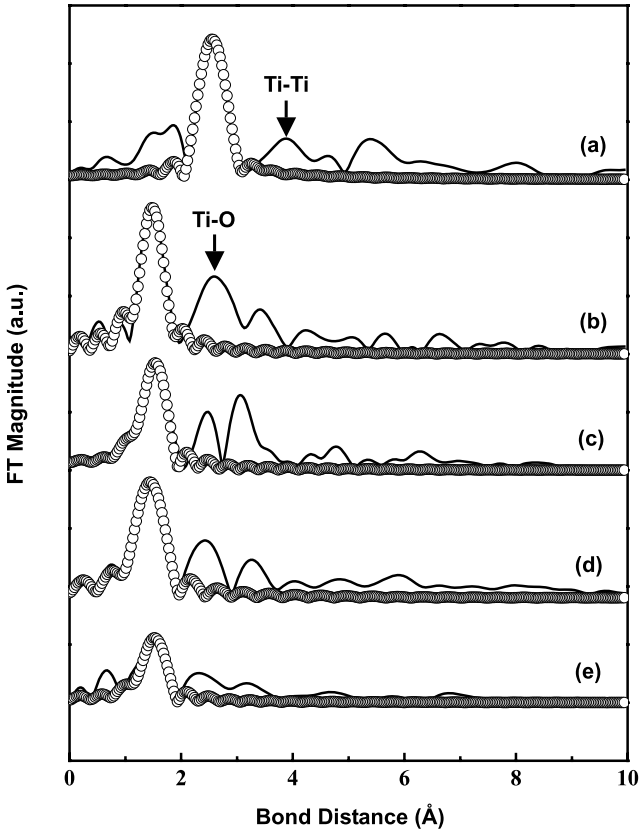

Fig. 5 Fourier transform (FT) of Ti K-edge EXAFS oscillation for (**a**) titanium, (**b**) anatase, (**c**) rutile, (**d**) titanate nanotube, and (**e**) TN. The best fittings of the EXAFS spectra are all represented by the *circle lines*

Table 2 Fine structural parameters of commercial Ti standards and as-synthesized nanotubular titanate or titania samples analyzed using EXAFS spectra

Ti type	Shell (1st)	CN[a] (±0.05 Å)	R (Å)[b] (±0.01 Å)	$\Delta\sigma^2$ (Å^2)[c]
Ti_2O_3 powder	Ti–O	3.02	2.01	0.0161
Anatase powder	Ti–O	3.98	2.89	0.0026
Rutile powder	Ti–O	4.04	1.94	0.0015
Titanate nanotube	Ti–O	1.98	1.95	0.0048
Titania nanotube	Ti–O	2.31	1.97	0.0046

[a]CN: Coordination number

[b]R: Bond distance

[c]σ: Debye-Waller factor

caused by random motion of surface atom on the small Ti particles instead of a true shortening of the bond length. Titanium oxide has distinct types of crystal structure included with the rutile and anatase, even though the bond distances are similar with each other around 1.94 Å and the coordination number is 4. However, the Debye-Waller factors ($\Delta\sigma^2$) of the rutile phase were much lower than the anatase phase of the TiO_2. Among the different By EXAFS spectra, the valency and framework of TN is Ti(IV) with octahedral structures. The results exposed that the TiO_2 anatase nanoparticles can be dissolved and changed into layer structures under strong alkaline (NaOH) conditions. The layer of TN further curling itself to reduce the Gibbs free energy was postulated and found. For calcination temperatures >400°C, the microstructure of TN might transform from nanotubes into nanoparticles accompanying with the sharp increase for the nanoparticle crystalline phase.

3.5 Analysis of adsorption isotherms for BG5 dye

Adsorption isotherms of the BG5 dye in solution at different temperatures are represented in Fig. 6. As seen the adsorption capacity of basic dyes on TN is largely perceptible to temperature changes and the isotherm is represented as type I (BG5 dye) (Brunauer 1944). Also, the change of adsorption isotherm type may be closely related to the effect of basic dyes adsorption on the pore structure stability of TN. In follows, the adsorption mechanism of BG5 dye from water solution onto TN surfaces is first examined with the aid of the Dubinin-Kaganer-Radushkevich (DKR) equation (Lin et al. 2002; Krishna et al. 2004). The DKR equation has the following form:

$$\ln Q = \ln Q_m - \beta\varepsilon^2 \tag{1}$$

where Q is the adsorption amount of BG5 in mol g^{-1}, Q_m (mol g^{-1}) the DKR monolayer capacity, β (mol^2 J^{-2}) a constant related to sorption energy, and ε is the Polanyi potential which is related to the equilibrium concentration as (since BG5 is easily soluble in water at 298 K, the solubility limit of Cs happens to be 1)

$$\varepsilon = RT\ln\left(\frac{1}{C}\right) \tag{2}$$

where T is the temperature and C is the equilibrium concentration of BG5. The slope and intercept of the plots of ln Q versus ε^2 give β and Q_m, respectively. The value of β is related to sorption energy, E, via the following relationship

$$E = \frac{-1}{\sqrt{-2\beta}} \tag{3}$$

The DKR parameters and E values for the adsorption of BG5 basic dye onto TN are presented in Table 3. The correlation coefficients (r^2) for linear regression analysis are close to unity. As shown in Table 3, the E values are found to be –14.98, –14.45, and –12.0 kJ mol^{-1} for BG5 adsorption at 25, 35, and 45°C, respectively. As expected, these values are of the order of an ion-exchange mechanism, in which the sorption energy lies within 8–16 kJ mol^{-1} (Lin et al. 2002). As shown in Fig. 6, the concentration of the adsorbed BG5

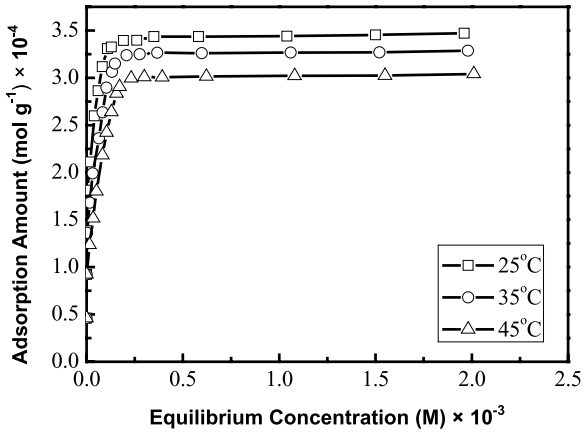

Fig. 6 Adsorption isotherms of the BG5 dye onto TN at different temperatures and constant pH = 4

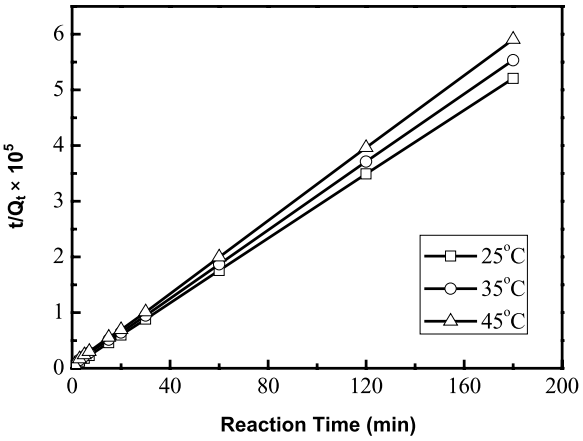

Fig. 7 Kinetic model of pseudo-second order reaction for the BG5 adsorption onto TN. The initial concentration and condition of the BG5 dye solution were 900 mg L^{-1} and pH = 4, respectively

Table 3 DKR parameters and E values of the BG5 dye adsorption onto TNs

T (°C)	Q_m (mol g^{-1}) × 10^{-3}	β (mol^2 J^{-2}) × 10^{-9}	E (kJ mol^{-1})
25	0.97	–2.22	–14.98
35	1.04	–2.39	–14.45
45	1.45	–3.46	–12.00

Note: The initial concentration and condition of BG5 dye solution were 900 mg L^{-1} and pH = 4, respectively

Table 4 Parameters of kinetic model of the BG5 dye adsorption onto TNs

T (°C)	Pseudo second-order model		
	k (g mol^{-1} min^{-1})	Q_e (mol g^{-1}) × 10^{-4}	R^2
25	2931.3	3.47	0.999
35	1943.2	3.28	0.999
45	1854.9	3.07	0.999

Note: The initial concentration and condition of BG5 dye solution were 900 mg L^{-1} and pH = 4, respectively

decreases with increased temperature at a given equilibrium concentration and the adsorption is an exothermic process. The temperature dependency of Henry's constant K obeys the van't Hoff equation (Ruthven 1984):

$$\frac{\mathrm{d}\ln K}{\mathrm{d}T} = \frac{\Delta H}{RT^2} \tag{4}$$

where R is the gas constant and T is the temperature (in Kelvin). Equation (4) can be integrated to yield $\ln K = \ln K_0 + (-\Delta H/RT)$. A plot of $\ln K$ versus $1/T$ will yield a straight line with a slope of $-\Delta H/R$. The heat of adsorption, calculated from the slope, is -33.9 ± 0.5 kJ mol^{-1} for the BG5 dye.

3.6 Analysis of adsorption kinetics

The effect of contact time on the amount of the BG5 dye adsorbed onto TN is measured at the optimum initial concentration and different temperatures. A simple kinetic analysis is performed with the aid of pseudo-second-order equation (Azizian 2004). In this equation, the value of the rate constant k can be calculated in the form:

$$\frac{\mathrm{d}Q_t}{\mathrm{d}t} = k(Q_e - Q_t)^2 \tag{5}$$

where Q_e and Q_t are the amount of dye adsorbed per unit mass of the adsorbent at equilibrium and time t, respectively. After definite integration by applying the initial conditions $Q_t = 0$ at $t = 0$ and $Q_t = Q_t$ at $t = t$, (5) becomes

$$\frac{t}{Q_t} = \frac{1}{kQ_e^2} + \frac{1}{Q_e}t. \tag{6}$$

Linear plots of the t/Q_t versus t with linear regression coefficients higher than 0.999 indicates the applicability of this kinetic equation and the pseudo-second nature of the adsorption process for basic dyes onto TN shown in Fig. 7. The kinetic parameters are listed in Table 4 obtained from the pseudo-second-order model and it is seen that the equilibrium adsorption capacity (Q_e) shows a slight decrease from with the increasing temperature. From the k values it is observed that for BG5, the temperature effect on the adsorption kinetics is insignificant.

In addition to the pseudo-second-order rate equation, the intraparticle diffusion model is commonly used for examining the steps involved during adsorption, described by external mass transfer (boundary layer diffusion) and intraparti-

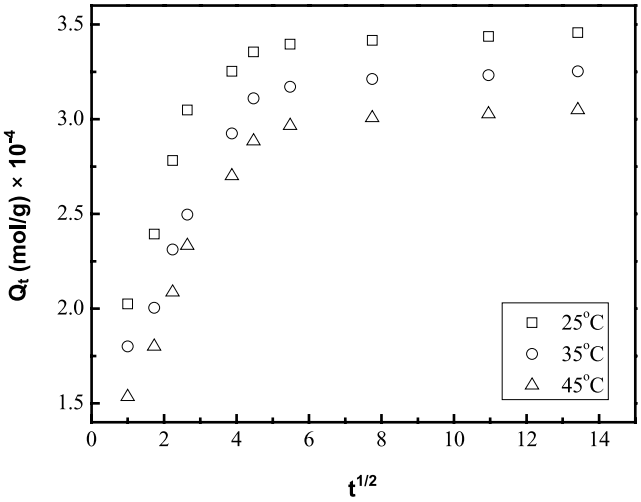

Fig. 8 The diffusion model plots for the adsorption of the BG5 dye onto TN. The initial concentration and condition of the BG5 dye solution were 900 mg L^{-1} and pH = 4, respectively

cle diffusion (Wang et al. 2006). The intraparticle diffusion model is expressed as:

$$Q_t = k_d t^{1/2} \tag{7}$$

where k_d is the diffusion coefficient. Figure 8 presents the typical plots for the adsorption of BG5 on TN using diffusion model. As shown in Fig. 8, the two-phase plot suggests that the adsorption process may possibly proceed by surface adsorption and intraparticle diffusion, namely, the initial curved portion of the plot indicates a boundary-layer effect while the second linear portion is due to intraparticle or pore diffusion. In addition, because the double nature of intraparticle diffusion plot confirms the presence of a boundary-layer effect and pore diffusion, the adsorption kinetic data can be further analyzed using Boyd kinetic expression (8) to determine the actual rate-controlling step involved in the dye adsorption process. In the present experiments, the initial high concentration and condition of BG5 dye solution were 900 mg L^{-1} and pH = 4, respectively. Moreover, because the nature of intraparticle diffusion plot confirms the presence of a boundary-layer effect and pore diffusion. The dependence of adsorption capacity Q_m on the temperature and adsorbate is inconsistent with the adsorption isotherms shown in Fig. 8, which may be due to the fact that the DKR equation is apparently obeyed in a high concentration range (Lin et al. 2002; Krishna et al. 2004).

Adsorption kinetic data can be further analyzed using Boyd kinetic expression (8) to determine the actual rate-controlling step involved in the BG5 dye adsorption process (Boyd et al. 1947).

$$G = 1 - \frac{6}{\pi^2}\exp(-Bt) \tag{8}$$

$$B = \frac{\pi D}{r^2} = \text{time constant} \tag{9}$$

Where D is the effective diffusion coefficient of adsorbates in adsorbent phase, r is the radius of adsorbent particle assumed to be spherical, and G is the fraction of solute adsorbed at different times t and given by

$$G = \frac{Q_t}{Q_e} \tag{10}$$

where Q_t and Q_e represent the amount adsorbed (mol g^{-1}) at time t and at infinite time. In this work, we take Q_e from the second-order kinetic model, as listed in Table 4. Substituting (10) into (8), the kinetic expression becomes

$$Bt = -0.4977 - \ln\left(1 - \frac{Q_t}{Q_e}\right). \tag{11}$$

Figure 9 represents that the calculated Bt values against t for BG5 at 25°C. In general, if the plot of Bt vs t is a straight line passing through the origin, the adsorption is governed by a particle-diffusion mechanism, otherwise it is governed by film diffusion (Vadivelan et al. 2005). As shown in Fig. 9, it is evident that the plots are not straight lines that pass through the origin, implying external mass transport mainly governs the rate of adsorption. It is noteworthy that this type of pattern is also found for the BG5 dyes adsorption on different adsorbents shown in Table 5. Comparison of the adsorption capacity of photocatalytic TN nanophase materials on other adsorbents without photocatalytic abilities, the residual BG5 dyes in solution can be further photocatalyzed onto TN that may be notably enhanced for the BG5 removal efficiency. Moreover, some published papers have also reported other adsorbents for dyes adsorption such as MCM-22 for methylene blue of 0.18 mmol g^{-1} at 303 K (Wang et al. 2006), rice husk for methylene blue of 0.11 mmol g^{-1} at 305 K (Vadivelan et al. 2005), activated carbon for methylene blue and methylene orange of 0.03 and 0.03 mg/g at 303 K respectively (Singh 2003), and fly ash for methylene blue of 0.02 mmol g^{-1} at 303 K (Kumar 2005). Therefore, the high potential of TN with both adsorptive and photocatalytic abilities for the removal of the BG5 dye contaminant from wastewaters suggests that further development would be warranted.

4 Conclusions

The current study represents the synthesis and characterization of TiO_2 nanotube structure materials. FE-SEM photographs showed that the formed nanotubes have a diameter of 10–30 nm and a length of several hundreds nanometers. Experimentally, TN synthesized by a simple hydrothermal treatment of crystallites formed a crystalline structure with

Table 5 Adsorption capacities of the BG5 dye in aqueous solutions onto different adsorbents

Adsorbent	Adsorption capacity (mol g^{-1}) $\times 10^{-4}$	Temperature (K)	Reference
Montmorillonite (BG5Ca-Mont.)[a]	10.46	298	Wang et al. (2004)
Montmorillonite (BG5Ti-Mont.)[b]	2.66	298	Wang et al. (2004)
MCM-41	32.5	298	Juang et al. (2006)
Titanate nanotube	8.91	298	Lee et al. (2008)
Titania nanotube	3.47	298	This work

Notes: [a]BG5Ca-Mont." and [b]BG5Ti-Mont." denote "BG5" adsorbed onto "Ca cation exchanged montmorillonite" and "Ti cation exchanged montmorillonite", respectively

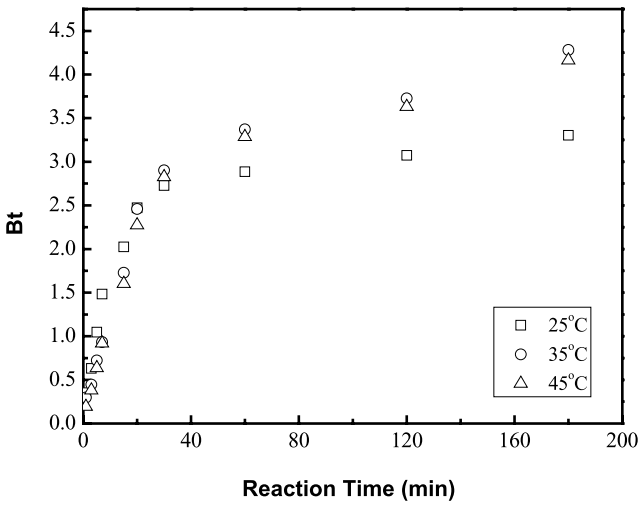

Fig. 9 Correlation between Bt and t for the BG5 dye adsorption onto TN. The initial concentration and condition of the BG5 dye solution were 900 mg L^{-1} and pH = 4, respectively

open-ended and multiwall morphologies. The XRD and N_2 adsorption isotherm techniques implied that acid washing could improve the TN specific surface area and the pore size distribution up to 292 $m^2\,g^{-1}$ and 40–60 nm, respectively. During the increasing time of acid washing, Na^+ of the titanate nanotube is replaced with H^+ to form hydrogen titanium oxide or hydrogen titanium oxide hydrate and that caused a decrease in the surface area of TN. In addition, the XRD diffraction patterns indicated that the formation of TN structure is much more stable after a 24 h acid washing process. By using EXAFS/XANES spectra, it is clearly seen that structure of the titanium oxide has distinct types of crystal structure included with the rutile and anatase even though the bond distances are similar with each other around 1.94 Å, with a coordination number of 4. In addition, TN is closer to the anatase specimen and much more correlated with the octahedral structure, including it's valency and framework of Ti(IV). Furthermore, TN may be an effective adsorbent for basic dye removal from aqueous solutions. The adsorption isotherm type I (BG5), which might be closely related to the effect of basic dyes adsorption on the pore structure stability of TN. Adsorption energy evaluated from DKR equation for the adsorption of BG5 onto TN showed that an ion-exchange mechanism was operative. Thermodynamic calculations indicated that the adsorption of basic dyes on TN was an exothermic process and the ΔH^0 for BG5 was -33.9 ± 0.5 kJ mol^{-1}. The adsorption kinetics followed the pseudo-second-order model and the external diffusion was the controlling process.

Acknowledgements The financial support of National Science Council (NSC-96-2211-E-155-022) of Taiwan, ROC is gratefully acknowledged.

References

Azizian, S.: Kinetic models of sorption: a theoretical analysis. J. Colloid Interface Sci. **276**, 47–52 (2004)

Berry, A.J., Walker, A.M., Hermann, J., O'Neill, H.S.C., Foran, G.J., Gal, J.D.: Titanium substitution mechanisms in forsterite. Chem. Geol. **242**, 176–186 (2007)

Bond, G.C.: Heterogeneous Catalysis-Principles and Applications, 2nd edn., p. 20. Oxford Science Publications, Oxford (1987)

Boyd, G.E., Adamson, A.W., Myers, L.S. Jr.: The exchange adsorption of ions from aqueous solutions by organic zeolites. II. Kinetics. J. Am. Chem. Soc. **69**, 2836–2848 (1947)

Brunauer, S.: The Adsorption of Gases and Vapours. Oxford University Press, London (1944)

Crini, G.: Non-conventional low-cost adsorbents for dye removal: a review. Bioresour. Technol. **97**, 1061–1085 (2006)

Cassano, A., Molinari, R., Romano, M., Drioli, E.: Treatment of aqueous effluents of the leather industry by membrane processes: a review. J. Membr. Sci. **181**, 111–126 (2001)

Chen, Q., Zhou, W., Du, G., Peng, L.: Trititanate nanotubes made via a single alkali treatment. Adv. Mater. **14**, 1208–1211 (2002)

Ho, K.Y., McKay, G., Yeung, K.L.: Selective adsorbents from ordered mesoporous silica. Langmuir **19**, 3019–3024 (2003)

Hsieh, C.T., Fan, W.S., Chen, W.Y., Lin, J.Y.: Adsorption and visible-light-derived photocatalytic kinetics of organic dye on Co-doped titania nanotubes prepared by hydrothermal synthesis. Sep. Purif. Technol. **67**, 312–318 (2009)

Inagaki, M., Kondo, N., Nonaka, R., Ito, E., Toyoda, M., Sogabe, K., Tsumura, T.: Structure and photoactivity of titania derived from nanotubes and nanofibers. J. Hazard. Mater. **161**, 1514–1521 (2009)

Juang, L.C., Wang, C.C., Lee, C.K.: Adsorption of basic dyes onto MCM-41. Chemosphere **64**, 1920–1928 (2006)

Kasuga, T.: Formation of titanium oxide nanotubes using chemical treatments and their characteristic properties. Thin Solid Films **496**, 141–145 (2006)

Kasuga, T., Hiramatsu, M., Hoson, A., Sekino, T., Niihara, K.: Titania nanotubes prepared by chemical processing. Adv. Mater. **11**, 1307–1311 (1999)

Kubo, T., Nakahira, A.: Local structure of TiO_2-derived nanotubes prepared by the hydrothermal process. J. Phys. Chem. C **112**, 1658–1662 (2008)

Kumar, K.V., Ramamurthi, V., Sivanesan, S.: Modeling the mechanism involved during the sorption of methylene blue onto fly ash. J. Colloid Interface Sci. **284**, 14–21 (2005)

Krishna, B.S., Mahadevaiah, N., Murty, D.S.R., Prakash, B.S.J: Surfactant immobilized interlayer species bonded to montmorillonite as recyclable adsorbent for lead ions. J. Colloid Interface Sci. **271**, 270–276 (2004)

Lee, C.K., Lin, K.S., Wu, C.F., Lyu, M.D., Lo, C.C.: Effects of synthesis temperature on the microstructures and basic dyes adsorption of titanate nanotubes. J. Hazard. Mater. **150**, 494–503 (2008)

Lin, S.H., Juang, R.S.: Heavy metal removal from water by sorption using surfactant-modified montmorillonite. J. Hazard. Mater. **92**, 315–326 (2002)

Lin, C., Lin, K.S.: Photocatalytic oxidation of toxic organohalides with TiO_2/UV: the effects of humic substances and organic mixtures. Chemosphere **66**, 1872–1877 (2007)

Lytle, F.W.: The EXAFS family tree: a personal history of the development of extended X-ray absorption fine structure. J. Synchrotron Radiat. **6**, 123–134 (1999)

Mohamed, M.M.: Acid dye removal: comparison of surfactant-modified mesoporous FSM-16 with activated carbon derived from rice husk. J. Colloid Interface Sci. **272**, 28–34 (2004)

Niu, H.Y., Wang, J.M., Shi, Y.L., Cai, Y.Q., Wei, F.S.: Adsorption behavior of arsenic onto protonated titanate nanotubes prepared via hydrothermal method. Microporous Mesoporous Mater. **122**, 28–35 (2009)

Pokhrel, D., Viraraghavan, T.: Treatment of pulp and paper mill wastewater—a review. Sci. Total Environ. **333**, 37–58 (2004)

Prado, A.G.S., Costa, L.L.: Photocatalytic decouloration of malachite green dye by application of TiO_2 nanotubes. J. Hazard. Mater. **169**, 297–301 (2009)

Ramakrishna, K.R., Viraraghavan, T.: Dye removal using low cost adsorbents. Water Sci. Technol. **36**, 189–196 (1997)

Ribeiro, C., Vila, C., Stroppa, D.B., Mastelaro, V.R., Bettini, J., Longo, E., Leite, E.R.: Anisotropic growth of oxide nanocrystals: insights into the rutile TiO_2 phase. J. Phys. Chem. C **111**, 5871–5875 (2007)

Ruthven, D.M.: Principles of Adsorption and Adsorption Processes. Wiley, New York (1984)

Ryuhei, Y., Yoshikazu, S., Susumu, Y.: Effects of synthetic conditions and heat-treatment on the structure of partially ion-exchanged titanate nanotubes. Mater. Chem. Phys. **91**, 409–416 (2005)

Seo, D.S., Lee, J.K., Kim, H.: Preparation of nanotube-shaped TiO_2 powder. J. Crystal Growth **229**, 428–432 (2001)

Singh, K.P., Mohan, D., Sinha, S., Tondon, G.S., Gosh, D.: Color removal from wastewater using low-cost activated carbon derived from agricultural waste material. Ind. Eng. Chem. Res. **42**, 1965–1976 (2003)

Sun, Z., Chen, Y., Ke, Q., Yang, Y., Yuan, J.: Photocatalytic degradation of cationic azo dye by TiO_2/bentonite nanocomposite. J. Photochem. Photobiol. A, Chem. **149**, 169–174 (2002)

Tomoko, K., Masayoshi, H., Akihiko, H., Toru, S., Koichi, N.: Formation of titanium oxide nanotube. Langmuir **14**, 3160–3163 (1998)

Tsai, C.C., Teng, H.: Nanotube formation from a sodium titanate powder via low-temperature acid treatment. Langmuir **24**, 3434–3438 (2008)

Uzunova-Bujnova, M., Dimitrov, D., Radevb, D., Bojinova, A., Todorovsky, D.: Effect of the mechanoactivation on the structure, sorption and photocatalytic properties of titanium dioxide. Mater. Chem. Phys. **110**, 291–298 (2008)

Vadivelan, V., Kumar, K.V.: Equilibrium, kinetics, mechanism, and process design for the sorption of methylene blue onto rice husk. J. Colloid Interface Sci. **286**, 90–100 (2005)

Wang, Y.Q., Hu, G.Q., Duan, X.F., Sun, H.L., Xue, Q.K.: Microstructure and formation mechanism of titanium dioxide nanotubes. Chem. Phys. Lett. **365**, 427–431 (2002)

Wang, C.C., Juang, L.C., Hsu, T.C., Lee, C.K., Lee, J.F., Huang, F.C.: Adsorption of basic dyes onto montmorillonite. Chemosphere J. Colloid Interface Sci. **273**, 80–86 (2004)

Wang, S., Li, S., Xu, L.: Application of zeolite MCM-22 for basic dye removal from wastewater. J. Colloid Interface Sci. **295**, 71–78 (2006)

Wang, D., Zhou, F., Liu, Y., Liu, W.: Synthesis and characterization of anatase TiO_2 nanotubes with uniform diameter from titanium powder. Mater. Lett. **62**, 1819–1822 (2008)

Weng, L.Q., Song, S.H., Hodgson, S., Baker, A., Yu, J.: Synthesis and characterization of nanotubular titanates and titania. J. Eur. Ceram. Soc. **26**, 1405–1409 (2006)

Wu, X., Ling, Y., Liu, L., Huang, Z.: Enhanced photoelectrocatalytic degradation of methylene blue on smooth TiO_2 nanotube array and its impedance analysis. J. Electrochem. Soc. **156**, 65–71 (2009)

Yu, J., Yu, H., Cheng, B., Trapalis, C.: Effects of calcination temperature on the microstructures and photocatalytic activity of titanate nanotubes. J. Mol. Catal. A, Chem. **249**, 135–142 (2006a)

Yu, J., Yu, H., Cheng, B., Zhao, X., Zhang, Q.: Preparation and photocatalytic activity of mesoporous anatase TiO_2 nanofibers by a hydrothermal method. J. Photochem. Photobiol. A, Chem. **182**, 121–127 (2006b)

Yu, J., Xiang, Q., Zhou, M.: Preparation, characterization and visible-light-driven photocatalytic activity of Fe-doped titania nanorods and first-principles study for electronic structures. Appl. Catal. B, Environ. **90**, 595–602 (2009)

Zhang, Y., Fu, W., Yang, H., Qi, Q., Zeng, Y., Zhang, T., Ge, R., Zou, G.: Synthesis and characterization of TiO_2 nanotubes for humidity sensing. Appl. Surf. Sci. **254**, 5545–5547 (2008)

Zhao, Q., Li, M., Chu, J., Jiang, T., Yin, H.: Preparation, characterization of Au (or Pt)-loaded titania nanotubes and their photocatalytic activities for degradation of methyl orange. Appl. Surf. Sci. **255**, 3773–3778 (2009)